JOURNAL OF SOLID STATE CHEMISTRY 86, 50–58 (1990)

Simple Band Model for $La_{1-x}Sr_xCoO_3$: Evidence from Electron Spectroscopy

J. P. KEMP,[1] D. J. BEAL, AND P. A. COX

Inorganic Chemistry Laboratory, South Parks Road, Oxford OX1 3QR, United Kingdom

Received June 1, 1989; in revised form January 3, 1990

Valence band photoelectron spectra and high resolution electron energy loss spectra for $La_{1-x}Sr_xCoO_3$ ($x \leq 0.5$) have been measured. The general appearance and variation with photon energy of the former may be interpreted in terms of the density of states arising from a simple semiempirical tight binding band structure calculation, for reasonable values of Hamiltonian matrix elements. The latter show a highly damped loss feature below 1 eV which may be assigned to a plasma oscillation whose frequency is overestimated by the same calculations, indicating a considerable enhancement of effective mass through correlation. Some care must, however, be taken in these analyses, since the samples show a mild segregation of strontium at the surface.

Introduction

The electronic structure of first row transition metal oxides has had a long history of study by both experimental and theoretical techniques, and is still today an area in which there is great activity, especially since the advent of high temperature superconductors (*1*). The often complex and diverse behavior shown by these compounds arises due to the fact that the various competing energies which affect electronic behavior (such as bandwidths, exchange energies, on-site electron–electron repulsion) are generally of a similar order of magnitude (*2*). The series $LaMO_3$ provide a nice illustration of this. All adopt the perovskite structure, or mild distortions of it, but there is an immense variation in electrical properties across the series, ranging from being semiconducting/metallic (M = Ti), through antiferromagnetic insulators (M = Cr, Mn, Fe), to a Pauli paramagnetic metal (M = Ni). This general pattern of behavior was rationalized by Goodenough (*2*), as being due to competition between d-bandwidths, which favor delocalization, and exchange/correlation energies, which favor localized, high-spin configurations.

$LaCoO_3$ occupies a unique place in this series, since both localized (low-spin $3d^6$) and itinerant (filled t_{2g} band) states give rise to an insulator or semiconductor. As it appears to lie on the border between localized ($LaFeO_3$) and itinerant ($LaNiO_3$) behavior, much effort has been devoted to resolving which case applies. Early work on conductivity (*3, 4*), Mössbauer spectroscopy (*4*), and PES (*5*) was interpreted in terms of a localized model. More recently, however, this view has been challenged by Thornton *et al.* (*6*), who interpret conductivity and

[1] To whom correspondence should be addressed.

0022-4596/90 $3.00

differential thermal analysis data on this and other rare earth cobaltates in terms of an itinerant model.

In this work, we present valence band photoelectron spectra at different photon energies, and show that they may be quantitatively interpreted in terms of a band model. We also present electron energy loss data for $LaCoO_3$ and strontium-doped samples, and show that these too may be interpreted using the same band structure, despite some complications due to mild surface segregation of strontium. We also show that correlation effects in this material are far from negligible, as is expected for a $3d$ transition metal oxide on the right-hand side of the series.

Experimental

Samples of $La_{1-x}Sr_xCoO_3$ ($0 \leq x \leq 0.5$) and also a sample of $SrCoO_{2.5}$ were prepared by intimately grinding an appropriate mixture of $La_2(C_2O_4)_3$, $SrCO_3$, and CoC_2O_4 in an agate mortar. This was then slowly raised to a temperature of 1150 K in air and held there for 15 hr to drive off all CO and CO_2. The resultant mixture of oxides was then reground, compacted at 10 ton force, and heated in air at 1350 K for 24 hr, followed by regrinding and annealing at 1150 K for up to 60 hr, to ensure the samples were not oxygen deficient. The products were characterized by powder diffraction, which yielded patterns in agreement with other workers (*7*), with no sign of other phases, and also by analysis for Co and Sr, which yielded compositions in close agreement with nominal ones. Following a report that separation into phase of different Sr content can occur at the higher doping levels (*8*), grains of the sample with $x = 0.5$ were analyzed by energy dispersive X-ray analysis in a JEOL 2000FX analytical electron microscope. No evidence for any such phase separation was seen, however.

All electron spectra were recorded in a VG ESCALAB 5 spectrometer, with an analyzer chamber equipped with twin anode X-ray source (for unmonochromatized Mg$K\alpha$ or Al$K\alpha$ radiation), a noble gas discharge lamp for UVPES, and an electron monochromator for HREELS, which provided a beam with energy variable from 5 to 100 eV and optimal FWHM around 15 meV. In order to obtain higher count rates, the resolution was deliberately degraded to ca. 75 meV in the studies of electronic losses.

The samples were finely ground and pressed into disks between optically flat tungsten carbide dies. The pellets were then secured to platinum sample trays using Pt clips and introduced into the spectrometer. Oxide surfaces often show extensive contamination due to surface carbonate and hydroxide, so in order to remove these without surface oxygen loss, the samples were heated in the spectrometer preparation chamber by radio-frequency induction to 1100 K under a pressure of 200 mbar of pure O_2 (predried by passage through a molecular sieve) for periods of 15 hr. They were then allowed to cool while the chamber was pumped down to 10^{-8} mbar, before being transferred to the analyzer chamber (base pressure below 10^{-10} mbar). Following this treatment, XPS showed that carbon contamination was negligible and losses due to OH stretch could not be detected by HREELS. Furthermore, the intensities of Sr $3d$, La $3d$, and O $1s$ ionizations, weighted by ionization cross sections (*9*) and electron mean free paths (*10*), gave a ratio $(I_{Sr} + I_{La}) : I_O$ close to 1 : 3 in all cases.

Results and Discussion

(*A*) *Surface Composition*

Figure 1 shows Mg$K\alpha$-excited XPS in the region of La $4d$ and Sr $3d$ ionizations for several samples, stripped of contributions from inelastic background and radiation

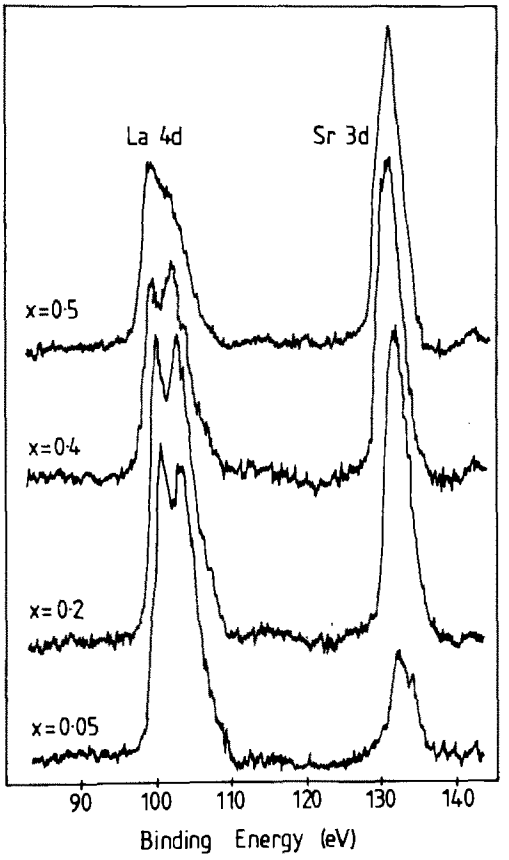

FIG. 1. Mg$K\alpha$-excited XPS of La 4*d* and Sr 3*d* region of $La_{1-x}Sr_xCoO_3$ for x = 0.5, 0.4, 0.2, and 0.05.

satellites. The ratio of cross section-weighted intensities is plotted in Fig. 2 as a function of composition. This data shows a smooth trend in surface composition, but also a marked enrichment of strontium at the surface. This will naturally mean that care is required in interpreting the results of any surface spectroscopies.

In order to provide some quantification of this it was assumed that enrichment only occurred in the topmost atomic layer of the material. The calculated proportion of strontium in surface A-sites is also shown in Fig. 2. Obviously, where the surface occupancy becomes greater than unity, some enrichment is also occurring in the second and subsequent layers of the solid. However, the general picture suggested is one where the surface A-sites, where there is possibly a reduced coordination number, and therefore a reduced Madelung potential, are preferentially occupied by the ion of lower charge, and lower layers, with a complete coordination environment, are affected to a much lower extent. This segregation has been observed previously in this system (*11*) by Tabata *et al.* These authors found a minimum in surface strontium content at $x = 0.2$, but since no form of annealing was employed in their measurements, it is likely that their surfaces were not properly in equilibrium with the bulk of the material.

The first two points on the graph may be used to estimate a heat of segregation, ΔH_S, via

$$\frac{\theta_s}{1-\theta_s} = \frac{\theta_b}{1-\theta_b}\exp(-\Delta H_s/RT),$$

where θ_s and θ_b are, respectively, the fractions of surface and bulk A-sites occupied

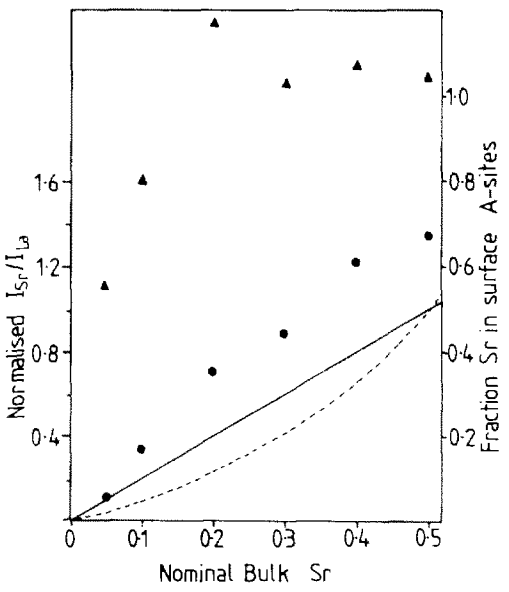

FIG. 2. Surface Sr/La content in $La_{1-x}Sr_xCoO_3$ from XPS (circles) and theoretical value (dashed line); data refers to left-hand scale. Surface A-site occupancy by Sr (triangles) and theoretical values (solid line); data refers to right-hand scale.

by Sr. The values are 26.1 and 29.8 kJ · mol^{-1} for $x = 0.05$ and $x = 0.1$ annealed at 1100 K. The close agreement between these again suggests that the surfaces are well equilibrated. It is unfortunately not possible to apply this equation to cases where $x \geq 0.2$, since here the value of $1 - \theta_s$ is rather less than the error involved in its estimation.

(B) Valence Band PES

Figure 3 shows valence band photoelectron spectra of $LaCoO_3$ excited by HeI (21.2 eV), HeII (40.8 eV), and Al$K\alpha$ (1486.6 eV) radiation. The ratio of cross sections

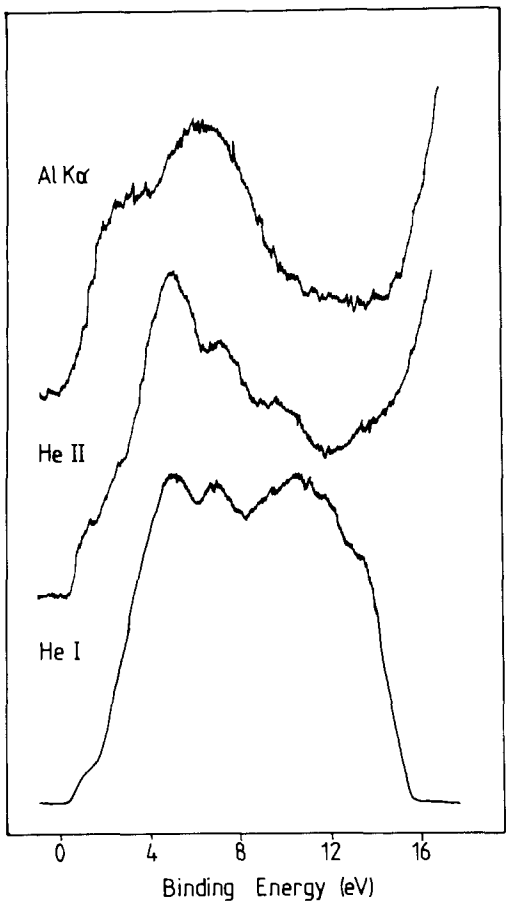

FIG. 3. Observed valence band photoelectron spectra of $LaCoO_3$, excited by unmonochromatized Al$K\alpha$ (1486.6 eV), HeII (40.8 eV), and HeI (21.2 eV) radiation.

Co(3d):O(2p) increases with photon energy and is equal to 15 (*9*) for Al$K\alpha$ radiation. Thus the latter reflects almost entirely ionizations from the metal. These lie in two bands, centered around 1.5 and 7.5 eV binding energy. This is rather unlike materials where the *d*-electrons are thought of as being localized, e.g., CoO; in this and similar materials, the valence region XPS show that most of the 3*d* spectral weight is concentrated in a narrow band near the Fermi energy, often with a satellite peak to higher binding energy (*12*).

The UVPE spectra show, rather, more structure. There is a peak at 7.3 eV binding energy which matches that in the XPS. A feature appears at 5.1 eV binding energy, becoming more prominent at lower photon energies. This must clearly be due to states where the electrons are being ionized almost entirely from O 2*p*. Finally, there is a step in the spectrum centered around 0.5 eV plus a slight shoulder at 2.5–3 eV, which increases in intensity with increasing photon energy, and matches the feature to lower binding energy in the XPS. For a perovskite AMO_3, where the transition metal M is d^6, the highest filled band is expected to arise from π-type overlap between O 2*p* and M $3d_{xz,yz,xy}$ orbitals. Such a band is essentially two-dimensional in nature, and the resulting density of states should possess a sharp onset and termination, and rise to a peak in between. The form of the UVPE spectra at low binding energy is very suggestive of such behavior, implying that the photoelectron spectra reflect ionization from a material with delocalized electrons, rather than a local Co $3d^6$ configuration. This is in direct conflict with previous interpretations of the photoelectron spectra of this material (*5*), but is supported by more recent DTA and conductivity studies (*6*).

To investigate further the similarity between the spectra and the expected DOS for a perovskite, a simple semiempirical tight binding calculation was performed,

TABLE I

DISPOSABLE MATRIX ELEMENT USED IN THE TIGHT-BINDING CALCULATION

Element	Value (eV)	
$\langle Co\ 3d_\pi \vert H \vert O\ 2p_\pi \rangle$	1.6	Two-center integrals
$\langle Co\ 3d_\sigma \vert H \vert O\ 2p_\sigma \rangle$	2.0	
$\langle Co\ 3d_\sigma \vert H \vert Co\ 3d_\sigma \rangle$	3.3	One-center integrals
$\langle Co\ 3d_\pi \vert H \vert Co\ 3d_\pi \rangle$	−1.5	
$\langle O\ 2p_\sigma \vert H \vert O\ 2p_\sigma \rangle$	−1.3	
$\langle O\ 2p_\pi \vert H \vert O\ 2p_\pi \rangle$	−1.7	

using essentially the same scheme as that employed by Mattheiss to interpolate between APW results on ReO_3 (*13*). The basis set excluded all orbitals on lanthanum and the slight rhombohedral distortion of the structure away from cubic (*7*) was ignored. A considerable number of parameters are needed to describe the various diagonal and off-diagonal elements of the Hamiltonian matrix. O–O nearest and next nearest neighbor interactions were fixed to be the same as in ReO_3. All M–M interactions were set to zero on the grounds that these are not large in ReO_3 or $KTaO_3$ (*14*), and are expected to be even smaller for $3d$ orbitals. The difference between the diagonal elements for O $2p\sigma$ and O $2p\pi$ was set to a similar value to that for ReO_3. This then leaves the only disposable parameters as the diagonal elements for O $2p\sigma$, Co $3d\sigma$, and $3d\pi$, and the Co–O σ- and π-interactions, though obviously the element for the σ-interaction must be the larger of the two. These were varied in order to produce a DOS with a band gap at the Fermi energy, and the correct occupied bandwidth, always bearing in mind the values used in calculations on other transition metal oxides. Table I shows the final set of values adopted. A point worth noting is that there is a large gap in energy between metal σ- and π-orbitals (necessary to give a band gap). In part this can be ascribed to crystal field effects, where repulsion from electrons on oxygen raises the energy of σ-type orbitals (*16*), but the main contribution is probably due to neglected interactions between O $2s$ and $3d\sigma$ (*15*). The metal $3d\pi$ levels are also very close in energy to the O $2p$ which will give rise to strong mixing of these.

Figure 4 shows the partial and full density of states for the system, calculated by a tetrahedral method. This may be divided into four regions. Above the Fermi energy is an unoccupied band of primarily Co $3d\sigma$ states. Between 0 and 4 eV binding energy is the upper (antibonding) half of the band formed from overlap of Co $3d\pi$ and O $2p\pi$ orbitals. This shows the expected form for a two-dimensional band, corresponding to the features observed in the UVPES at low binding energy. There is then a sharp peak

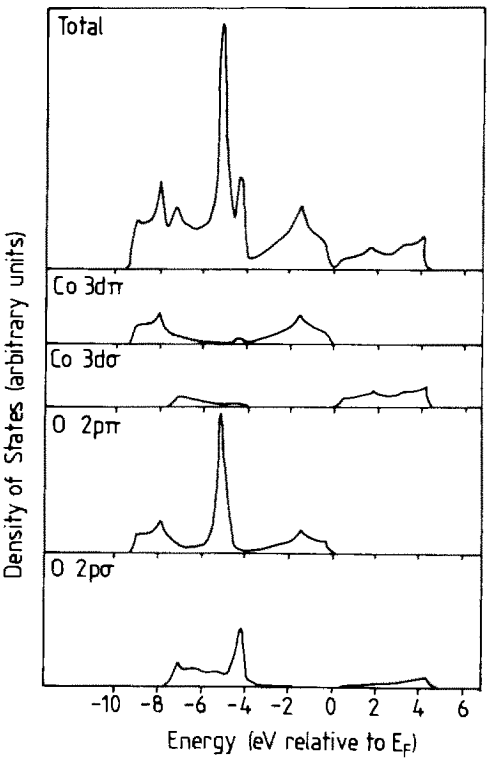

FIG. 4. Calculated density of states for $LaCoO_3$. Upper panel, total DOS, followed by partial DOS for Co $3d\sigma$, Co $3d\pi$, O $2p\sigma$, and O $2p\pi$.

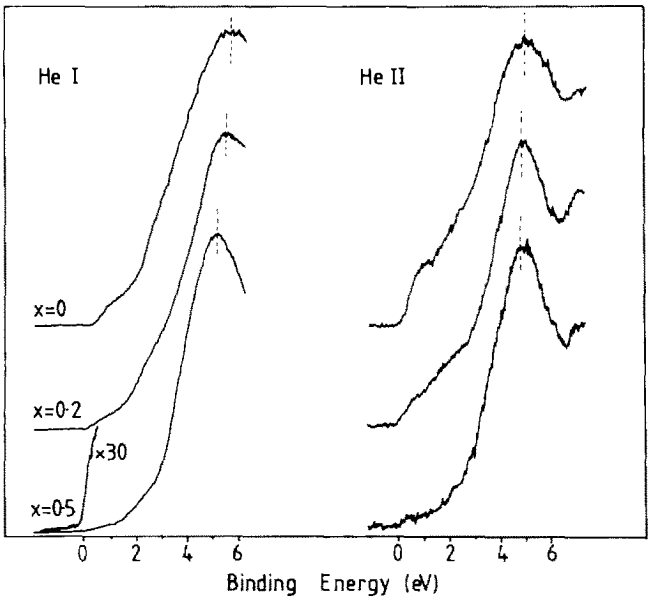

FIG. 5. HeI- and HeII-excited UVPES of $La_{1-x}Sr_xCoO_3$ for $x = 0.5$, 0.2, and 0. Dotted line indicates shift in nonbonding O $2p$ states.

at 5.2 eV consisting of nonbonding O $2p$ orbitals. This clearly matches the peak in the photoelectron spectra, and the intensity of ionizations from these states would be expected to decrease dramatically with increasing photon energy. Finally, there is a region spanning 6 to 9 eV binding energy, which consists of the bonding halves of the π- and σ- bands. The occupied density of states on Co thus falls into two lobes, which ties in with the valence XPE spectrum.

If the bands are assumed to be rigid, then strontium doping of the material will give rise to upward band-bending. As strontium is only divalent, and lanthanum trivalent, removal of electrons from the CoO_3 host lattice is necessary to balance charges. Thus the valence band shows an upward shift toward the Fermi energy (which in our instrument is pinned to that of the spectrometer, for conducting samples). This is observable in the UVPE spectra shown in Fig. 5, where the nonbonding O $2p$ levels are seen to shift upwards with increasing doping, by approximately 0.2 eV for $x = 0.2$ and 0.5 eV for $x = 0.5$. Theoretical values may be derived from the density of states and are listed in Table II. All are larger than the observed values, but by a constant amount. This arises through the finite width (0.2 eV) used for the intervals for calculating the density of states. This gives rise to a low tail extending into the band gap, which results in large values for the band-bending for only small doping levels. It is seen, however, that the difference in band-bend-

TABLE II

CALCULATED BAND-BENDING IN $La_{1-x}Sr_xCoO_3$

x	Band-bending (eV)
0.1	0.35
0.2	0.45
0.3	0.52
0.4	0.60
0.5	0.66

ing between $x = 0.2$ and $x = 0.5$ is correct, within the limits of the accuracy of measurement (± 0.1 eV).

It is clear from Fig. 5, however, that in the region close to the Fermi energy, the tight-binding density of states becomes a poorer representation of the photoemission spectra, as the strontium content increases. The effect observed is a decrease in intensity between 0 and 3 eV binding energy, which is more pronounced at higher photon energies (see Fig. 5), suggesting that the effect occurs more at cobalt than at oxygen. We interpret this as showing that although the electrons are best described as itinerant in $LaCoO_3$, they are still highly correlated. This will be seen to a greater extent at Co than at O since we expect the on-site repulsion, U, to be greater for a $3d$ orbital than for $2p$. In $LaCoO_3$ itself, such effects are not observed, as only a single hole is present in a filled band after photoionization. We are thus dealing with a one-particle problem, and the one-particle DOS gives a fair representation of the PE spectrum. With increasing doping with Sr, however, the number of holes in the band increases, and many-particle effects become more pronounced, leading to a progressive breakdown of the one-electron picture. In a future publication (*17*), we hope to discuss the effects of correlation on the spectra of this material in greater detail.

Also noteworthy is the fact that despite being metallic, neither the $x = 0.2$ nor $x = 0.5$ compounds appear to possess a Fermi edge in their UVPE spectra. One does in fact become visible for the $x = 0.5$ sample, on an expended scale (see Fig. 5), but is much smaller than the density of states suggested by the calculations. In part this can again be ascribed to correlation, which leads to a shift of the density of states seen in photoemission away from E_F (see e.g., (*18*). A further major contribution is likely to be electron–phonon interactions, which lead to the holes in the material being better described as polarons. In the sudden approximation, the photohole will be introduced as a bare particle, and will thus correspond to a superposition of vibrational states of the ionized system, in which the ground state (which alone can yield photoelectrons at the Fermi energy) has only small weight.

(*C*) *Electron Energy Loss Spectra*

Figure 6 shows EEL spectra for $LaCoO_3$ and $La_{0.5}Sr_{0.5}CoO_3$, measured in specular mode at 25 eV incident beam energy. In the strontiated sample, a shoulder appears on the side of the elastic peak, up to 1 eV loss energy. As the strontium content is reduced, the shoulder decreases in intensity and moves into the elastic peak, and the spectra evolve into that of $LaCoO_3$. For clarity, the spectra of the samples with intermediate strontium content are presented in Fig. 5 as the difference between the actual spectrum and that of $LaCoO_3$. The feature appears in these as a distinct peak for $x \geq 0.3$, and may be assigned to a highly damped plasmon, which increases in frequency as the strontium content, and thus carrier concentration increases. A previous report (*7*) claimed that for $x = 0.5$, there is a minimum in the reflectivity at 2.3 eV which the authors assigned to a plasmon. No features are seen in EELS at this energy, and since the report did not show the actual reflectance spectrum, we are unable to comment further on this.

Provided the lifetime does not change greatly in the series, the feature should evolve from an undefined shoulder, when $\Omega_p < 1/\tau$, to a peak once $\Omega_p > 1/\tau$. This suggests a value for $1/\tau$ in the region of 0.5 eV, which is about a factor of two greater than other doped metal oxides, e.g., Na_xWO_3 (*19*) or $Sb_xSn_{1-x}O_2$ (*20*). The shortness of the lifetime is indicative of narrower bands and considerably greater correlation in $LaCoO_3$ than in the other systems, which is to be expected from the

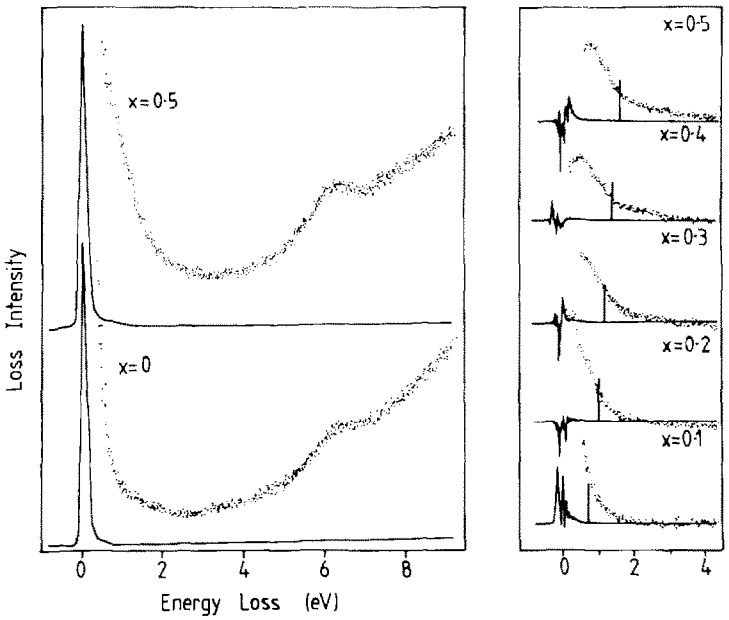

FIG. 6. EEL spectra of $La_{1-x}Sr_xCoO_3$. Left-hand panel compares $x = 0$ and $x = 0.5$. Right-hand panel shows difference spectra between strontiated samples and $LaCoO_3$ as a function of x. Solid vertical line indicates calculated plasma frequency.

relative spatial extent of 3*d* orbitals, compared with 5*d* or 5*s* and 5*p*. Conductivity data may also be used to calculate a lifetime, via (*21*)

$$\tau = 1/(\rho\Omega_p^2\varepsilon_0\varepsilon_\infty)$$

The resistivity for $0.2 \leq x \leq 0.4$ lies in the range $4\text{–}8 \times 10^{-5}$ Ω m at room temperature (*7*), which for a plasmon energy of 0.5 eV gives a value for $1/\tau$ in the range 0.5–1.0 eV, which is the same order of magnitude as that deduced from the EEL spectra.

It is important to consider surface composition at this point, however. Since compounds with greater than 20% strontium have all surface A-sites filled by Sr (qv), a sample of a phase containing 100% Sr was synthesized and studied. $SrCoO_3$ itself is not stable in air at 1100 K, but loses oxygen down to approximately $SrCoO_{2.5}$ (*22*). When the EEL spectrum of a sample of the latter was measured, it was virtually identical to that of $LaCoO_3$, suggesting that the EEL spectra should not be greatly influenced by a surface phase containing 100% Sr. Additionally, the penetration depth, given by

$$\lambda = v_\perp/\omega,$$

for a 25 eV beam and 0.5 eV loss energy, is equal to 2 nm, or six lattice spacings. Thus the spectra should not be too sensitive to changes in composition in the topmost layer, and should largely reflect bulk carrier concentration.

The plasma frequency may also be calculated from the band structure scheme above using the formula (*23*)

$$\Omega_p^2 = (2/3\varepsilon_0\varepsilon_\infty)e^2\hbar^2N(E_f)v^2(E_f),$$

where $N(E_f)$ is the density of states per spin at the Fermi energy, and $v^2(E_f)$ is the electronic velocity squared at the Fermi energy, averaged over the Fermi surface. For many oxide materials, the optical dielectric constant ε_∞ is around 4, so this value was

used. The results are shown as tick marks on the difference spectra in Fig. 6, and although there is some difficulty in precisely locating the experimental loss features, the calculated values appear in all cases to be roughly a factor of two too large. This is consistent with an enhancement of the effective mass over the band value due to correlation. This may be discussed in terms of the model proposed by Brinkman and Rice (*24*), where it is given by

$$m_{\text{eff}}/m = [1 - (U/U_0)^2]^{-1}.$$

Here, U is the on-site Coulomb energy, and U_0 the value of this quantity required to open a gap at the Fermi energy. For an effective mass enhancement of four times (since $\Omega_p \propto m^{-1/2}$), this implies that the carriers in this material are strongly correlated and only barely in the itinerant regime. This is also found to be the case for related materials, such as $LaNiO_3$ (*25*), and suggests that the same may be true of carriers in the high-T_c copper oxide superconductors.

Conclusions

In conclusion, we have shown that the results from electron spectroscopies of the valence electrons in $LaCoO_3$ and strontiated analogs may be interpreted quantitatively using a simple band model for the system. It is, however, evident that holes introduced into the highest filled band could not be described by nearly free electron theory. Thus $La_{0.5}Sr_{0.5}CoO_3$ is ferromagnetic (*7*) (rather than Pauli paramagnetic) and the carriers have a high effective mass and short lifetime, all of which are indicative of a regime where the bandwidth is greater than on-site repulsion, but not substantially so. In a future publication (*17*), we hope to address the effect of correlation in this material more closely.

References

1. J. G. Bednorz and K. A. Müller, *Z. Phys. B* **64,** 189 (1986).
2. J. B. Goodenough, *Prog. Solid State Chem.* **5,** 276 (1971).
3. R. R. Heikes, R. C. Miller, and R. Mazelsky, *Physica* **30,** 1600 (1964).
4. V. G. Bhide, D. S. Rajoria, G. Rama Rao, and C. N. R. Rao, *Phys. Rev. B* **6,** 1021 (1972).
5. A. F. Orchard and G. Thornton, *J. Electron Spectrosc. Relat. Phenom.* **22,** 271 (1981).
6. G. Thornton, F. C. Morrison, S. Partington, B. C. Tofield, and D. E. Williams, *J. Phys. C* **21,** 2871 (1988).
7. V. G. Bhide, D. S. Rajoria, C. N. R. Rao, G. Rama Rao, and V. G. Jadhao, *Phys. Rev. B* **12,** 2832 (1975).
8. P. M. Raccah and J. B. Goodenough, *J. Appl. Phys.* **39,** 1209 (1968).
9. J. H. Scofield, *J. Electron Spectrosc. Relat. Phenom.* **8,** 129 (1976).
10. D. R. Penn, *J. Electron. Spectrosc. Relat. Phenom.* **9,** 29 (1976).
11. K. Tabata, I. Matsumoto, and S. Kohiki, *J. Mater. Sci.* **22,** 1882 (1987).
12. G. K. Wertheim and S. Hüfner, *Phys. Rev. Lett.* **28,** 1028 (1972).
13. L. F. Mattheiss, *Phys. Rev.* **181,** 987 (1969).
14. L. F. Mattheiss, *Phys. Rev. B* **6,** 4718 (1972).
15. L. F. Mattheiss, *Phys. Rev. B* **2,** 3918 (1970).
16. C. J. Ballhausen, "Introduction to Ligand Field Theory," McGraw–Hill, New York (1962).
17. J. P. Kemp, D. J. Beal, and P. A. Cox, *J. Phys. Condens. Matter,* submitted for publication.
18. P. A. Cox, R. G. Egdell, J. B. Goodenough, A. Hamnett, and C. C. Naish, *J. Phys. C* **16,** 6221 (1983).
19. R. G. Egdell, H. Innes, and M. D. Hill, *Surf. Sci.* **149,** 33 (1985).
20. R. G. Egdell, W. R. Flavell, and P. Tavener, *J. Solid State Chem.* **51,** 345 (1984).
21. N. W. Ashcroft and N. D. Mermin, "Solid State Physics," Chap. 1, Holt–Saunders, Tokyo (1976).
22. M. Arjomand and D. J. Machin, *J. Less-Common Met.* **61,** 133 (1978).
23. H. Cohen, *Philos. Mag.* **3,** 762 (1958).
24. W. F. Brinkman and T. M. Rice, *Phys. Rev. B* **2,** 4302 (1970).
25. J. P. Kemp and P. A. Cox, *Solid State Commun.*, submitted for publication.